NeuroImage: Clinical 37 (2023) 103316

Contents lists available at ScienceDirect

NeuroImage: Clinical

journal homepage: www.elsevier.com/locate/ynicl

Cerebellar gray matter alterations predict deep brain stimulation outcomes in Meige syndrome

Bin Liu [a,b], Zhiqi Mao [b], Zhiqiang Cui [b], Zhipei Ling [b], Xin Xu [b], Kunyu He [a,b], Mengchu Cui [a,b], Zhebin Feng [a,b], Xinguang Yu [b,c,*], Yanyang Zhang [b,c,*]

[a] Medical School of Chinese PLA, Beijing, PR China
[b] Department of Neurosurgery, Chinese PLA General Hospital, Beijing, PR China
[c] Neurosurgery Institute, Chinese PLA General Hospital, Beijing, PR China

ARTICLE INFO

Keywords:
Meige syndrome
Cerebellum
Gray matter volume
Biomarker
Deep brain stimulation

ABSTRACT

Background: The physiopathologic mechanism of Meige syndrome (MS) has not been clarified, and neuroimaging studies centering on cerebellar changes in MS are scarce. Moreover, even though deep brain stimulation (DBS) of the subthalamic nucleus (STN) has been recognized as an effective surgical treatment for MS, there has been no reliable biomarker to predict its efficacy.

Objective: To characterize the volumetric alterations of gray matter (GM) in the cerebellum in MS and to identify GM measurements related to a good STN-DBS outcome.

Methods: We used voxel-based morphometry and lobule-based morphometry to compare the regional and lobular GM differences in the cerebellum between 47 MS patients and 52 normal human controls (HCs), as well as between 31 DBS responders and 10 DBS non-responders. Both volumetric analyses were achieved using the Spatially Unbiased Infratentorial Toolbox (SUIT). Further, we performed partial correlation analyses to probe the relationship between the cerebellar GM changes and clinical scores. Finally, we plotted the receiver operating characteristic (ROC) curve to select biomarkers for MS diagnosis and DBS outcomes prediction.

Results: Compared to HCs, MS patients had GM atrophy in lobule Crus I, lobule VI, lobule VIIb, lobule VIIIa, and lobule VIIIb. Compared to DBS responders, DBS non-responders had lower GM volume in the left lobule VIIIb. Moreover, partial correlation analyses revealed a positive relationship between the GM volume of the significant regions/lobules and the symptom improvement rate after DBS surgery. ROC analyses demonstrated that the GM volume of the significant cluster in the left lobule VIIIb could not only distinguish MS patients from HCs but also predict the outcomes of STN-DBS surgery with high accuracy.

Conclusion: MS patients display bilateral GM shrinkage in the cerebellum relative to HCs. Regional GM volume of the left lobule VIIIb can be a reliable biomarker for MS diagnosis and DBS outcomes prediction.

1. Introduction

Meige syndrome (MS) is a type of segmental cranial dystonia, manifesting as a bilateral involuntary contraction of the orbicularis oculi muscles at the early stage, followed by the progressive involvement of perioral muscles, jaw, tongue, pharyngeal, and cervical muscles (Pandey and Sharma, 2017). It can be classified into three categories according to the involved craniofacial muscles: blepharospasm, oromandibular dystonia, and blepharospasm-oromandibular dystonia, among which blepharospasm combined with oromandibular dystonia is regarded as the complete type of MS (Ma et al., 2021). Its low incidence and the absence of megascopic brain lesions on routine imaging complicate the disclosure of the neurobiological mechanisms underlying MS.

Neuroimaging studies, with the ability to detect microstructural

Abbreviations: MS, Meige syndrome; HCs, human controls; GM, gray matter; WM, white matter; GPi, globus pallidus internal; STN, subthalamic nucleus; VBM, voxel-based morphometry; LBM, lobule-based morphometry; SUIT, Spatially Unbiased Infratentorial Template; ROC, receiver operating characteristic; BFMDRS-M, Burke-Fahn-Marsden Dystonia Rating Scale movement subscale; BFMDRS-D, Burke-Fahn-Marsden Dystonia Rating Scale disability subscale; TIV, total intracranial volume; FWE, family-wise error; AUC, area under the curve; LOOCV, leave-one-out cross validation; ROI, region of interest; CTC, cerebello-thalamo-cortical circuit; FC, functional connectivity.

* Corresponding authors at: Department of Neurosurgery, Chinese PLA General Hospital, 28 Fuxing Road, Haidian District, Beijing 100853, China.
E-mail addresses: yuxinguang_301@163.com (X. Yu), sjwkzyy@163.com (Y. Zhang).

https://doi.org/10.1016/j.nicl.2023.103316
Received 12 August 2022; Received in revised form 21 November 2022; Accepted 2 January 2023
Available online 4 January 2023

alterations or connectivity abnormalities in vivo, play an indispensable role in clarifying the pathogenesis of MS. Early studies focused on the abnormalities of basal ganglia. However, recent studies indicated that dystonia is a kind of network disorder (Jinnah et al., 2017). Modern imaging methods, such as voxel-based morphometry (VBM) (Zheng et al., 2012), tract-based spatial statistics (Pinheiro et al., 2015), functional activity or connectivity (Battistella et al., 2017; Bianchi et al., 2019), and graph theory analysis (Chirumamilla et al., 2019; Jiang et al., 2019), have identified structural and functional abnormalities in multiple regions (basal ganglia, cerebellum, cortex, thalamus, and brainstem), as well as the disturbance of their reciprocal connectivity, indicating the involvement of the cortico-striato-pallido-thalamo-cortical and the cerebello-thalamo-cortical (CTC) circuits.

The cerebellum, as an indispensable portion of the sensorimotor circuit, has been proven with compelling evidence to be engaged in the physiopathological substrate of dystonia (Morigaki et al., 2021), especially of MS (Pandey and Sharma, 2017). Firstly, cerebellar abnormalities in MS have been identified in gray matter (GM) changes (Obermann et al., 2007; Piccinin et al., 2014a; Ramdhani et al., 2014; Tomic et al., 2021), white matter (WM) (Ramdhani et al., 2014; Yang et al., 2014), structural connectivity (Chirumamilla et al., 2019), neural activity (Nguyen et al., 2020; Zhou et al., 2013), functional connectivity (FC) (Fang et al., 2021; Jochim et al., 2018), and metabolic activity (Hutchinson et al., 2000; Liu et al., 2021). Secondly, the lesions in the cerebellum accounted for a large part of secondary blepharospasm patients (Khooshnoodi et al., 2013). Thirdly, about half of dystonic animal models were built on cerebellar abnormalities (Bologna and Berardelli, 2018; Pizoli et al., 2002; White and Sillitoe, 2017). Moreover, both resting-state functional MRI (Buckner et al., 2011) and task-related functional MRI (King et al., 2019; Xue et al., 2021) demonstrated that the majority of the cerebellum could map to distinct cerebral association networks in an orderly manner, hinting at the fact that the cerebellum is involved in a wide array of motor and non-motor functions. Likewise, MS is also characterized by a combination of motor and non-motor components (such as anxiety, depression, and sleep disorders) (Ma et al., 2021; Valls-Sole and Defazio, 2016). Thus, it is rational to investigate the cerebellum solely to unravel the physiopathologic mechanism. However, among all the previous neuroimaging studies about MS, only one applied a specialized cerebellar template (Piccinin et al., 2014b), and most studies used a whole-brain template, which is not conducive to finding minor changes in the cerebellum. Additionally, due to the heterogeneous methodologies and inclusion criteria of patients, the results of these studies were inconsistent. Most of these studies were degraded by their small sample sizes or mixed MS with other types of dystonia together for analysis, leaving an ambiguous pattern of alterations in MS.

At present, no gold standard test is available for the diagnosis of MS, and the current identification of MS relies solely on clinical symptoms. A reliable diagnostic biomarker is lacking, which is predisposed to confusing diagnosis and diagnostic delay. As to the treatment of MS, deep brain stimulation (DBS) has been widely regarded as a robust therapy, especially for those late-stage individuals who have failed initial therapy of botulinum toxin. Nonetheless, the efficiency of DBS, whether the stimulation target is globus pallidus internal (GPi) or the subthalamic nucleus (STN), varies across MS patients (Vagefi et al., 2008; Zhan et al., 2018). Reliable preoperative predictors to guide therapeutic decisions and to select appropriate surgery candidates have not been defined. Even though some retrospective studies suggested several clinical variables (baseline severity, disease duration, or stimulation targets) might be related to the prognosis of DBS surgery, such variables were unreliable and likely to become insignificant in other studies (Wang et al., 2019b). Furthermore, the question of if and how some MRI-based GM metrics can predict the outcomes of DBS surgery has not yet been addressed so far.

From this background, we combined two complementary methods together —— VBM (Ashburner and Friston, 2000; Good et al., 2001) and lobule-based morphometry (LBM), aiming to clarify the differences in GM volume between MS patients and normal human controls (HCs), as well as between DBS responders and DBS non-responders. Of note, all analyses were achieved using the Spatially Unbiased Infratentorial Template (SUIT) atlas, which outperformed the conventional whole-brain templates by preserving the anatomical details of the cerebellum and allowing for an improved alignment of cerebellar subregions (Diedrichsen, 2006; Diedrichsen et al., 2009). Additionally, we performed correlation analyses to identify significant clinical factors related to GM changes. Finally, we used receiver operating characteristic (ROC) analyses to see if the GM volumetric biomarkers could be a robust biomarker for MS diagnosis and a reliable predictor for DBS outcomes.

2. Materials and methods

2.1. Participants

A total of 47 MS patients (22 male and 25 female; mean age = 56.77 ± 8.44 years; all right-handed) who underwent DBS surgery (4 GPi-DBS and 43 STN-DBS) at the Chinese People's Liberation Army General Hospital from October 2015 to December 2021 were enrolled in the study. Fifty-two age- and sex-matched HCs (21 male and 31 female; mean age = 54.17 ± 10.12 years; all right-handed) were recruited from patients' spouses or the local community (Table 1). An experienced neurologist diagnosed MS patients, and only idiopathic or inherited MS patients were included. Patients were excluded if they had taken any neuropsychiatric drugs before the onset of MS, had a relative history of craniofacial trauma, began to suffer from MS prior to age 20, had obvious dystonic symptoms affecting their trunk and limbs (to keep the group homogeneity), or had any contraindications to MRI scanning. Those who had received botulinum toxin treatment were recruited at least three months after their last injection. A comprehensive neurological examination was performed to ensure neither MS patients nor HCs had a history of other neurological, psychiatric or metabolic disorders.

All MS patients underwent bilateral STN-DBS surgery after careful preoperative examinations. An intraoperative stimulation trial during wakefulness was conducted to test surgical response further. If specific adverse reactions occurred, the electrode position would be readjusted accordingly. An intraoperative MRI was arranged for each DBS patient to ensure the exact location of the implanted DBS electrodes.

The severity of dystonia was quantified preoperatively and postoperatively at the 6-month to 1-year follow-up (mean follow-up time = 8.5 months) by the Burke-Fahn-Marsden Dystonia Rating Scale movement (BFMDRS-M) and disability (BFMDRS-D) subscales (Burke et al., 1985). All patients were assessed by one professional neurologist to keep the unified scoring criteria. According to the classification criteria used by previous studies (Horisawa et al., 2018; Pauls et al., 2017; Tian et al., 2021; Wang et al., 2019a), the patients could be binarized into DBS responders (≥30% BFMDRS-M improvement rate) and DBS non-responders (<30% BFMDRS-M improvement rate). Regarding the contrast of DBS responders vs DBS non-responders, two patients were lost during follow-up, and four GPi-DBS patients were excluded to avoid the confounding effect of the stimulation target. Finally, 41 STN-DBS patients (31 DBS responders, 10 DBS non-responders) were involved in the final analysis (Table 1).

All subjects signed informed consent before participating, and the local ethics committee of the Chinese People's Liberation Army General Hospital approved his study.

2.2. Data acquisition

A set of 3.0 T MRI scanning systems with an 8-channel head coil (Discovery MR750, General Electric) was introduced to acquire images from all subjects. A three-dimensional T1 weighted structural image was acquired using a sagittal fast spoiled gradient-echo sequence (TR: 6.7

Table 1
Demographics and clinical variables of participants.

Group	MS (n = 47)	HCs (n = 52)	p^a	STN-DBS		p^b
				Responders (n = 31)	Non-responders (n = 10)	
Sex (male/female)	22/25	21/31	0.520	14/17	3/7	0.633
Age (years)	56.77 ± 8.44	54.17 ± 10.12	0.172	55.55 ± 8.46	60.40 ± 8.81	0.126
Education years	8.91 ± 3.66	9.25 ± 3.76	0.655	9.13 ± 3.74	10.10 ± 2.89	0.458
Disease duration (years)	5.20 ± 5.06	–	–	4.67 ± 4.79	6.85 ± 5.79	0.132
Follow-up time (months)	8.50 ± 2.34*	–	–	8.69 ± 2.35	7.90 ± 2.34	0.290
Pre-BFMDRS-M	12.48 ± 5.59*	–	–	11.71 ± 5.17	14.85 ± 6.43	0.101
Post-BFMDRS-M	5.06 ± 4.88*	–	–	3.16 ± 2.68	10.95 ± 5.56	**<0.001**
BFMDRS-M improvement (%)	57.75 ± 29.97*	–	–	68.22 ± 20.92	25.30 ± 15.00	**<0.001**
Pre-BFMDRS-D	3.51 ± 1.86*	–	–	3.48 ± 1.86	3.60 ± 1.96	0.744
Post-BFMDRS-D	1.22 ± 1.68*	–	–	0.65 ± 1.28	3.00 ± 1.56	**<0.001**
BFMDRS-D improvement (%)	62.87 ± 50.96*	–	–	82.39 ± 31.98	2.33 ± 52.43	**<0.001**

Values are shown as mean ± SD. p values are calculated using the two-tailed independent sample t-test or the Mann-Whitney U test, except for sex tested using the chi-square test. p^a values represent the differences between MS and HCs, and p^b values represent the differences between DBS responders and DBS non-responders. Significant p values at $p < 0.05$ (2-tailed) are reported in bold. Abbreviations: MS, Meige Syndrome; HCs, human controls; STN, subthalamic nucleus; DBS, deep brain stimulation; BFMDRS-M, Burke-Fahn-Marsden Dystonia Rating Scale movement subscale; BFMDRS-M, Burke-Fahn-Marsden Dystonia Rating Scale disability subscale.
* calculated among the 41 STN-DBS MS patients.

ms, TE: 2.9 ms, flip angle: 7°, FOV: 256 × 256 mm^2, number of slices: 192, slice thickness: 1 mm with no gap). Prior to imaging processing, all images were inspected in a blinded fashion to assure image quality and the absence of visible brain pathology. Scans with evident head motion artifacts or poor gray/white matter differentiation were excluded.

2.3. Image volumetric analysis

At the beginning, each T1 image was displayed on the Statistical Parametric Mapping (SPM12) software (http://www.fil.ion.ucl.ac.uk/spm), and the image origin was reset at the anterior commissure. Subsequently, by using the SUIT toolbox (V3.5) (https://www.diedrichsenlab.org/imaging/suit.htm) implemented in SPM12, the infratentorial structures of each image were isolated and segmented into cerebellar GM and WM in terms of the tissue probability maps. Meanwhile, a cerebellar isolation mask was generated, which, if necessary, was hand-corrected via the MRIcroGL software (https://www.nitrc.org/projects/mricrogl). Next, the cerebellar GM and WM probability maps in the individual space were normalized into the SUIT atlas using the Diffeomorphic Anatomical Registration Through Exponentiated Lie Algebra (DARTEL) algorithm (Ashburner, 2007), along with the step of modulation to grant within-voxel volume preservation. The resultant images were filtered using the function of image inhomogeneity correction in the Computational Anatomy Toolbox (CAT12, http://www.neuro.uni-jena.de/cat).

For VBM, all normalized and modulated images were smoothed with a 4 mm full-width at half-maximum smoothing kernel. An absolute threshold masking of 0.2 was used to avoid edge effects at the GM border. The resulting parametric maps were projected onto a two-dimensional representation of the cerebellar cortex via the Flatmap generator in the SUIT toolbox. Anatomical localizations were determined according to the probabilistic MRI atlas of the human cerebellum (Diedrichsen et al., 2009).

For LBM, the SUIT atlas was resliced into the native space of each subject by applying the inverse flowfield and affine transformation derived from the above normalization step. Due to the lack of corresponding high-resolution T2 images or functional MRI data, we omitted the evaluation of subcortical cerebellar nuclei. Finally, the volumes of 28 lobules were computed with the code provided by Diedrichsen's lab (https://www.diedrichsenlab.org/imaging/suit_faqs.htm). Moreover, we summated their hemispheric and vermian portions, yielding the volumes of 10 lobules: I-IV, V, VI, Crus I, Crus II, VIIb, VIIIa, VIIIb, IX, and X (see Supplementary Fig. 2A). The total cerebellar lobular volume was calculated for each subject as the sum of the 10 lobules. Additionally, the total intracranial volume (TIV) was also estimated in SPM12 as a nuisance variable in the subsequent statistical analyses to remove the effect of individual head size.

2.4. Statistical analyses

Group differences for demographic variables were probed by the independent two-tailed two-sample t-test (for age and educational level), the nonparametric Mann–Whitney U test (for disease duration, follow-up years, and BFMDRS-M/D scores), and the chi-square test (for sex), with a significance level set at $p < 0.05$.

For cerebellar VBM, group differences in both comparisons were tested by the general linear model (implemented in SPM12) with age, sex, TIV, and educational years as covariates, thresholded at $p < 0.001$ at the voxel level first and then FWE-corrected ($p < 0.05$) at the cluster level. The corresponding first eigen variate (mean GM volume) was extracted from the surviving clusters for the subsequent analysis. For LBM, group differences were investigated by the analysis of covariance (ANCOVA) to remove the effects of age, sex, TIV, and educational level, with a significance level set at $p < 0.005$, Bonferroni corrected for multiple comparisons (0.05/10, as the number of tested cerebellar lobules).

Moreover, we examined the relationships between the regional or lobular GM volumetric metrics and clinical variables (disease duration, preoperative BFMDRS-M/D scores, postoperative BFMDRS-M/D scores, and BFMDRS-M/D improvement rates) among the 41 STN-DBS MS patients. We only investigated the correlations for those GM areas showing significant group differences in VBM and LBM to limit the number of correlations. For each metric, a partial correlation analysis was performed after adjusting for age, sex, TIV, and educational level, at a significance level of $p < 0.0083$, Bonferroni corrected for multiple comparisons (0.05/6, as the number of tested clinical scores). Further, to visualize their linear relationships, we calculated the unstandardized residuals of GM metrics and clinical scores to remove the effect of confounders and plotted the partial correlation scatter diagrams with means + unstandardized residuals.

Finally, the ROC analyses were conducted to see to what extent the GM measurements of significant clusters or lobules can distinguish MS patients from HCs and forecast the outcomes of STN-DBS surgery. We used the mean GM volume of each significant cluster/lobule to perform ROC analyses. Also, we combined cluster 1–4 (four clusters) together as a whole and extracted the mean GM volume of this new mask to see its classification ability that was evaluated by the area under the curve (AUC). Besides, we referred to the method of leave-one-out cross-validation (LOOCV) to validate the accuracy of each cluster/lobule. The sensitivity, specificity, accuracy, and p values corresponding to the

optimal cutoff points in the ROC curves were also reported. All analyses were carried out using the Statistical Package for Social Science (SPSS V.26.0).

3. Results

3.1. Participant characteristics

Table 1 summarizes the demographic and clinical data. There were no significant differences in sex, age, and educational level between MS patients and HCs. For the comparison between STN-DBS responders (n = 31) and STN-DBS non-responders (n = 10), no significant differences were detected in sex, age, educational level, disease duration, follow-up time, and preoperative BFMDRS-M/D scores, whereas significant discrepancies were unearthed in postoperative BFMDRS-M/D scores and BFMDRS-M/D improvement rates ($p < 0.001$).

3.2. VBM analyses

We identified significant cerebellar GM volume atrophy in MS patients compared to HCs. These survival clusters (named cluster 1, cluster 2, cluster 3, and cluster 4, respectively) were localized in the bilateral lobule Crus I (with an extension to the lobule VI), bilateral lobule VIIb, bilateral lobule VIIIa, and VIIIb (Fig. 1A).

Moreover, we detected lower cerebellar GM volume in the left lobule VIIIb (named cluster 5) in DBS non-responders compared to DBS responders (Fig. 1B). Of note, most of cluster 5 overlaps with cluster 3 (see Supplementary Fig. 1), indicating its dual role in both comparisons. All detailed information is summarized in Table 2.

Table 2
Anatomical localization of significant clusters identified in both VBM analyses.

Cluster number	Cluster size (voxels)	Peak T	Peak MNI coordinate (mm)			Anatomical label (SUIT template)
			x	y	z	
MS (n = 47) < HCs (n = 52)						
1	425	−7.16	−28	−41	−37	Left Cerebellar Lobule Crus I
2	522	−6.63	22	−66	−47	Right Cerebellar Lobule VIIb Right Cerebellar Lobule VIIIa
3	919	−7.69	−19	−46	−51	Left Cerebellar Lobule VIIIa Left Cerebellar Lobule VIIIb Left Cerebellar Lobule VIIb
4	916	−7.65	38	−48	−33	Right Cerebellar Lobule VI Right Cerebellar Lobule Crus I
DBS responders (n = 31) > DBS non-responders (n = 10)						
5	322	4.87	−24	−45	−57	Left Cerebellar Lobule VIIIb

The significance level of all clusters is set at $p < 0.001$ at the voxel level first and then FWE-corrected ($p < 0.05$) at the cluster level. Abbreviations: MS, Meige Syndrome; HCs, human controls; VBM, voxel-based morphometry; DBS, deep brain stimulation; SUIT, Spatially Unbiased Infratentorial Template.

3.3. LBM analyses

Table 3 summarizes the detailed results of LBM analyses. No significant difference was found between MS patients and HCs in the total lobular volume of the cerebellum ($p = 0.068$). In terms of each lobule, significant volumetric atrophy was identified in the lobule VIIb ($p = 0.002$), VIIIa ($p = 0.002$), and VIIIb ($p = 0.001$) in MS patients.

Similarly, no group difference was yielded between DBS responders and DBS non-responders in the total lobular volume of the cerebellum ($p = 0.757$). In terms of each lobule, DBS non-responders had smaller GM volume in lobule VIIIb than DBS non-responders ($p = 0.039$), though this result failed to survive the multiple comparisons.

3.4. Correlation analyses

With sex, age, TIV, and educational level regressed out, neither the volumes of all surviving clusters nor the significant lobules correlated with disease duration, preoperative BFMDRS-M/D scores, or postoperative BFMDRS-M/D scores. However, the BFMDRS-M improvement rate positively correlated with the mean GM volume of cluster 5 ($r = 0.522$, $p = 0.001$), cluster 3 ($r = 0.444$, $p = 0.005$), and lobule VIIIb ($r = 0.440$, $p = 0.006$) (Fig. 2A-C). Moreover, a significant positive relationship also existed between the mean GM volume of cluster 5 and the

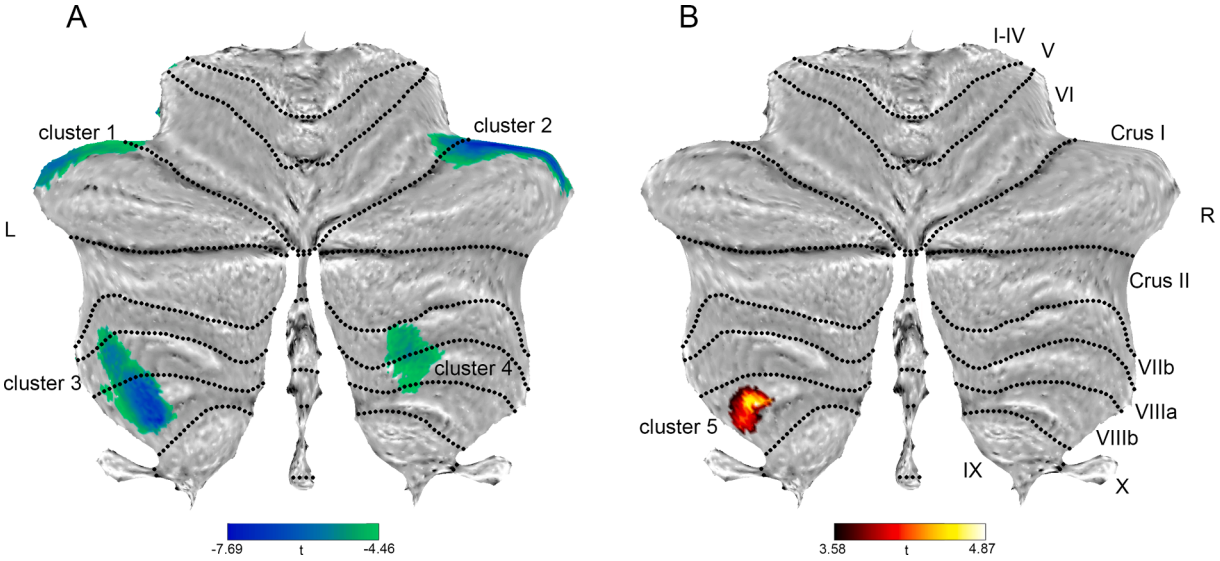

Fig. 1. VBM results projected onto the flatmap of the human cerebellum. A) Regions showing reduced GM volume in MS patients compared to HCs (named cluster 1, cluster 2, cluster 3, and cluster 4, respectively). B) Regions showing increased GM volume in DBS responders compared to DBS non-responders (named cluster 5). Color bars denote the t values. The black dotted lines on the flatmap separate the human cerebellum into 10 lobules. Abbreviations: VBM, voxel-based morphometry; FWE, family-wise error; GM, gray matter; DBS, deep brain stimulation.

Table 3
Lobular GM volumes in both LBM analyses.

	MS (n = 47)	HCs (n = 52)	p^a	STN-DBS		p^b
				Responders (n = 31)	non-responders (n = 10)	
Total lobular cerebellum	114.25 ± 10.67	117.62 ± 8.31	0.068	115.90 ± 11.24	109.95 ± 8.38	0.757
Lobule I–IV	6.76 ± 0.61	6.69 ± 0.54	0.396	6.88 ± 0.64	6.51 ± 0.39	0.602
Lobule V	8.08 ± 0.68	8.04 ± 0.64	0.569	8.18 ± 0.73	7.94 ± 0.51	0.767
Lobule VI	18.31 ± 1.53	18.96 ± 1.37	0.012	18.39 ± 1.64	18.11 ± 1.18	0.269
Lobule Crus I	24.76 ± 2.35	25.42 ± 1.88	0.160	25.01 ± 2.46	24.22 ± 2.04	0.765
Lobule Crus II	18.69 ± 2.01	18.93 ± 1.46	0.607	18.94 ± 2.13	17.80 ± 1.65	0.835
Lobule VIIb	9.68 ± 1.07	10.26 ± 0.80	**0.002**	9.82 ± 1.11	9.16 ± 0.89	0.483
Lobule VIIIa	10.68 ± 1.19	11.32 ± 0.89	**0.002**	10.87 ± 1.21	10.05 ± 0.10	0.353
Lobule VIIIb	8.45 ± 0.98	8.97 ± 0.72	**0.001**	8.69 ± 0.10	7.88 ± 0.75	**0.039**
Lobule IX	7.15 ± 0.96	7.28 ± 0.68	0.463	7.40 ± 0.96	6.67 ± 0.80	0.291
Lobule X	1.68 ± 0.18	1.75 ± 0.15	0.035	1.72 ± 0.20	1.61 ± 0.15	0.567

Lobular GM volumes (in milliliter) are expressed as mean ± SD. p^a values represent the differences between MS and HCs ($p < 0.005$, Bonferroni corrected), and p^b values represent the differences between DBS responders and DBS non-responders ($p < 0.05$, no multiple comparisons). All comparisons are corrected by age, sex, and TIV. Significant p values are reported in bold.
Abbreviations: MS, Meige Syndrome; HCs, human controls; GM, gray matter; LBM, lobule-based morphometry; STN, subthalamic nucleus; DBS, deep brain stimulation.

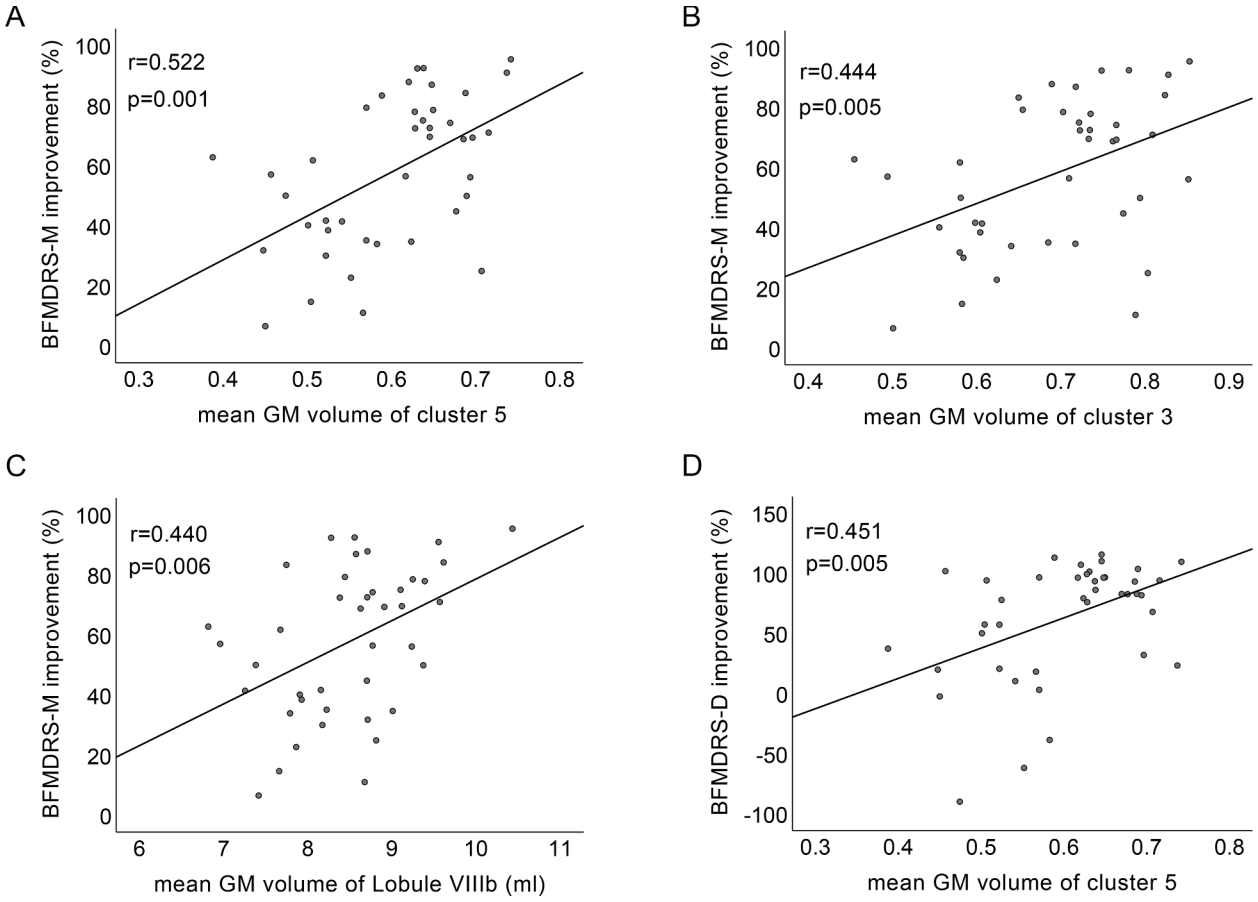

Fig. 2. Results of partial correlation analyses. A), Linear correlation between the mean GM volume of cluster 5 and BFMDRS-M improvement rate. B), Linear correlation between the mean GM volume of cluster 3 and BFMDRS-M improvement rate. C), Linear correlation between the mean GM volume of lobule VIIIb and BFMDRS-M improvement rate. D), Linear correlation between the mean GM volume of cluster 5 and BFMDRS-D improvement rate. Abbreviations: GM, gray matter; BFMDRS-M, Burke-Fahn-Marsden Dystonia Rating Scale movement subscale; BFMDRS-D, Burke-Fahn-Marsden Dystonia Rating Scale disability subscale.

BFMDRS-D improvement rate (r = 0.451, p = 0.005) (Fig. 2D).

3.5. ROC analyses

Regarding diagnostic performance, the combination of cluster 1–4 had the highest classification potency (AUC = 0.960, sensitivity = 91.49%, specificity = 88.46%, LOOCV-accuracy = 87.88%) (Fig. 3A, Supplementary Table 1). Each individual cluster had similar classification ability with AUC ranging from 0.836 to 0.869.

Regarding predictive performance, the mean GM volume of cluster 5 presented a reliable classification ability (AUC = 0.848, sensitivity = 87.10%, specificity = 80%, LOOCV-accuracy = 80.49%) (Fig. 3B, Supplementary Table 1). See Supplementary Table 1 for more information.

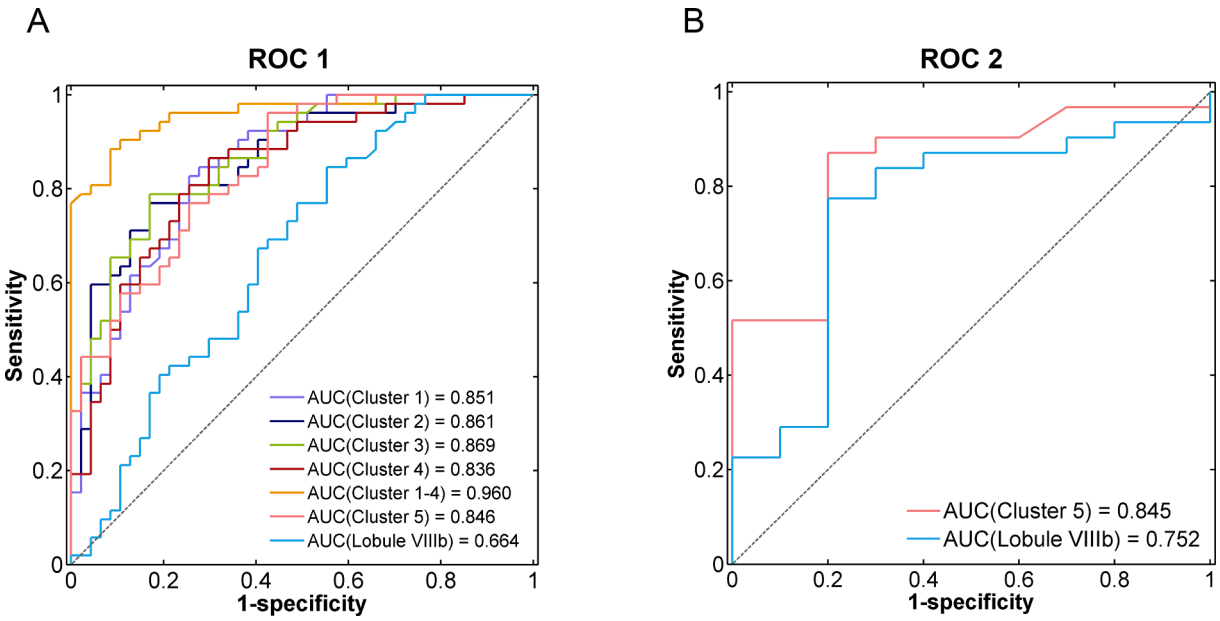

Fig. 3. Results of ROC analyses. A), ROC curves of the mean GM volume of significant clusters/lobule to distinguish MS patients from HCs. B), ROC curves of the mean GM volume of cluster 5 and lobule VIIIb to predict the outcomes of STN-DBS surgery. Abbreviations: ROC, receiver operating characteristic; MS, Meige syndrome; HCs, human controls; GM, gray matter; AUC, area under the curve.

4. Discussion

In this article, we identified an underlying pattern of GM atrophy mainly localized in the posterior lobe of the cerebellum on both sides in MS patients as compared to HCs. Also, we detected lower GM volume in the left lobule VIIIb in DBS non-responders relative to DBS responders. Furthermore, the GM volumetric parameters of the significant regions positively correlated with the BFMDRS-M/D improvement rates. Remarkably, the results of both morphometric methods (VBM and LBM) and both comparisons (MS vs HCs and DBS responders vs DBS non-responders) converged on the left lobule VIIIb, in which the mean GM volume of cluster 5 could be a reliable biomarker for MS diagnosis and STN-DBS outcomes prediction. To the best of our knowledge, the sample size of the MS group is the largest so far, and this is the first study to use MRI-based GM parameters to predict DBS efficacy in MS patients.

4.1. The cerebellar GM alterations in MS

The GM, as the aggregation of the cell body of neurons, is the main territory to process information, where billions of synapses interact with each other. Given that maladaptive synaptic plasticity and cortical hyperexcitability have been linked to the pathogenesis of MS (Ma et al., 2021), probing into GM alterations should be the first choice for us to decipher this intricate syndrome. To date, most of the VBM studies on craniocervical dystonia have also found significant GM alterations in the cerebellum. Obermann et al. (2007) firstly identified GM density increase in the left cerebellar culmen in blepharospasm patients, followed by Piccinin et al. (2014a) who found significant GM volume reduction in the cerebellar vermis IV/V and Ramdhani et al. (2014) who detected cerebellar GM volume increase in bilateral lobule VIIa in cervical dystonia and blepharospasm patients. Additionally, a recent study discovered significant GM atrophy in the posterior lobe of the cerebellum (left lobule Crus I, left lobule VIIIb, and right lobule Crus II) in patients of craniocervical dystonia relative to HCs (Tomic et al., 2021), which was analogous to our VBM results.

However, there exist several caveats in previous VBM studies. First, owing to the low incidence and the concomitant relationship between MS and cervical dystonia, most VBM studies combined them into craniocervical dystonia for analysis. In fact, the two types of dystonia phenotypes are different diseases, and they showed distinct patterns of microstructural disruptions when compared directly (Berman et al., 2018). So those studies using craniocervical dystonia as a whole may not reflect the accurate GM alterations in MS. Second, these studies used a whole-brain template, and the whole-brain multiple comparisons could conceal some subtle alterations in the cerebellum. This could explain why another two VBM studies with only MS patients included failed to find cerebellar GM changes (Liu et al., 2020; Martino et al., 2011). By now, only one study (Piccinin et al., 2014b) used a specific infratentorial template (SUIT) to investigate GM changes in the cerebellum, and they concluded that GM increased in the anterior lobe of the cerebellum and the brainstem but deceased in the posterior lobe of the cerebellum in craniocervical dystonia. This finding was partly in line with our results, and the reason why we did not identify GM increase in the cerebellum is probably that we only enrolled MS patients, whereas they mixed MS with cervical dystonia as a whole for analysis. Third, these studies were all VBM analyses, with no region of interest (ROI) -based analyses as a complement. VBM can reveal microregional GM alterations in an unbiased, prior hypothesis-independent manner, while the ROI-based analysis provides more interpretable metrics anatomically and may be more statistically robust. If combined, the two complementary approaches will yield more convincing results. Finally, the findings of these studies were inconsistent and even contradictory, which necessitated well-designed studies with larger sample sizes. By contrast, our study compensates for these shortcomings by focusing only on MS patients, applying a specific cerebellar template, incorporating VBM and LBM analyses, and involving a larger sample size. Therefore, our findings should be an important supplement and update to previous studies.

4.2. Microstructural changes in the cerebellum: Cause or consequence?

Although a large collection of cerebellar microstructural changes have been identified, the question of whether these changes are primary for the pathogenesis of dystonia or secondary to long-term dystonic movement remains unsolved (Malone et al., 2014). What we have detected in this article is no exception. In view of the lack of any relationships between GM changes and disease duration or symptom severity, we hypothesize that the shrinkage in the posterior lobe of the cerebellum can be explained as an etiological mechanism of cortical

hyperexcitability.

Specifically, the direct cause of cerebellar GM shrinkage is probably the loss of Purkinje neurons. Some neuropathological studies in blepharospasm (Fagan et al., 2021) and cervical dystonia (Prudente et al., 2013) have revealed a distinct reduction of Purkinje neurons in the cerebellum. As the only efferent fibers of the cerebellar cortex, the axons of Purkinje neurons connect with the deep cerebellar nuclei where most of the new fibers, via the relay of the ventrolateral thalamus, project to the interneurons in the sensorimotor cortices (Middleton and Strick, 1994; Morigaki et al., 2021; Voogd, 2003), constituting the CTC pathway. Through this pathway, we hypothesize that the reduction of efferent neural impulses caused by the atrophy of the cerebellar GM lowers the excitability of inhibitory interneurons and induces cortical disinhibition, which has been recognized as the primary physiological substrate of MS. This hypothesis is in accordance with previous neurophysiological studies. Popa et al. (2013) documented that cerebellar cortex excitation elicited by transcranial magnetic stimulation can interfere with the increase in M1 excitability elicited by paired-associative stimulation, while cerebellar cortex inhibition would facilitate it. Another neurophysiological study found that a lower GM density in the cerebellar hemispheres correlated with higher excitability in the primary motor cortex in dystonia patients (Fecikova et al., 2018). Indeed, except cerebellar cortex, CTC fiber impairment can also increase cortical excitability and induce the occurrence of MS. Argyelan et al. (2009) found that the integrity of CTC fiber tracts was reduced in dystonia patients compared to healthy volunteers, and the reduction positively correlated with the increase of activation response in the primary motor cortex. Mantel et al. (2022) also revealed a significant fractional anisotropy reduction within the CTC tract projecting to the right motor and left occipital cortex in MS patients relative to HCs.

Of course, considering the etiological heterogeneity of MS and the multiple cerebellar functions, we cannot draw a definitive causal conclusion according to the present findings. More in-depth physiological and multi-model neuroimaging studies, preferably with longitudinal designs, are needed to validate the causal relationship between the cerebellar microstructural alterations and the pathogenesis of MS.

4.3. The role of lobule Crus I, VIIb, VIIIa, VIIIb

We consider that the GM atrophy in lobule VIII (VIIIa and VIIIb) detected in this article corresponds to the motor symptoms of MS. Intrinsic functional studies have proved that the cerebellum has double motor representations —— an inverted representation in lobule V and VI and a second upright representation in lobule VIII (Buckner, 2013; Buckner et al., 2011). Further, according to a multi-domain task battery (MDTB) functional parcellation (King et al., 2019), the significant cluster (cluster 5) in lobule VIIIb is fully localized in the posterior associative motor region (region 4), which is responsible for action observation, motor planning, and divided attention (see Supplementary Fig. 2B). All these three functions are impaired in MS patients since the eyelids spasm or apraxia of eyelids opening can interfere with their visuospatial ability and attention, and then influence the motor comprehension and motor planning. Moreover, Luo et al. (2022) found lower dynamic FC between the lobule VIII and the primary motor cortex in blepharospasm patients compared to HCs and hemifacial spasm patients, and from this, they claimed that lobule VIII might play a crucial role in triggering the development of blepharospasm. All the evidence verifies the motor role of lobule VIII in MS.

The GM atrophy in lobule Crus I and VIIb detected in this article corresponds to the non-motor symptoms of MS. Previous FC analyses have found that lobule Crus I/Crus II are consistently activated during cognitive tasks (Xue et al., 2021). In light of the brain network identified by Buckner et al. (2011), the significant regions (cluster1 and cluster2) in bilateral Crus I identified in this article are both associated with the salience/ventral attention network, which is responsible for the adjustment of attention and the rapid switchover of different networks. Accordingly, MS patients, due to their eyelids spasm, have difficulty in evaluating the surrounding circumstances in real-time, making the transition of attention retarded. For lobule VIIb, most FC studies connected it with the dorsal/ventral attention network and the control network (Buckner et al., 2011; King et al., 2019; Xue et al., 2021), indicating its involvement in working memory and motor control. Moreover, several neuroimaging studies put lobule VIIb and VIIIa together for analysis. They demonstrated that the cerebellar lobule VIIb/VIIIa was functionally associated with the cortical dorsal attention network in a load-dependent way and participated in the tasks of visual working memory (Brissenden et al., 2016, Brissenden et al., 2018, Brissenden and Somers, 2019, Brissenden et al., 2021). It is common for MS patients to have problems with visual working memory owing to their eyelids spasm (Romano et al., 2014).

4.4. Biomarker for MS diagnosis and STN-DBS outcomes prediction

In general, a good biomarker should be capable of identifying the presence of disease, tracking progression, and foreseeing treatment response (Hohenfeld et al., 2018). In this article, the mean GM volume of cluster 5 identified by VBM can not only distinguish MS patients from HCs but serve as a reliable biomarker for STN-DBS outcomes prediction. Moreover, the mean GM volume of lobule VIIIb identified by LBM can also predict the STN-DBS efficacy with a moderate accuracy rate. Although the AUC value of LBM-based metrics is lower than that of VBM-based metrics (Fig. 3), the former has the advantages of simplifying the image processing steps and making the results more understandable anatomically.

As for the diagnosis of dystonia, the GM morphological network properties (Li et al., 2021), brain resting-state FC (Battistella et al., 2016; Pan et al., 2021; Pan et al., 2019), local field potentials in the GPi (Zhu et al., 2018) have been recognized as latent biomarkers to distinguish dystonic patients from HCs with satisfactory accuracy and sensitivity. Notably, a study compared the performance of anatomical, diffusional, and functional biomarkers, concluding that GM volume outperformed functional metrics and contributed more to the disease classification (Schouten et al., 2016). Therefore, the most recommended method is to choose GM volume as a diagnostic biomarker.

As for the DBS treatment of MS, a notable caveat is that some dystonic patients respond very well while others do not (Vagefi et al., 2008). This situation necessitates a reliable preoperative outcome predictor to guide therapeutic decisions and select appropriate surgery candidates. So far, several clinical biomarkers have been proven to be associated with the prognosis of DBS surgery for craniocervical dystonia patients, such as preoperative severity of disease (Wang et al., 2019a; Wang et al., 2019b), age at surgery (Hua et al., 2020), disease duration (Isaias et al., 2008), and electrodes position (Tian et al., 2021; Yao et al., 2019). In addition, some neurophysiological parameters, such as the average firing rates within GPi (Tian et al., 2021), the peak theta oscillatory activity within GPi (Neumann et al., 2017), and the volume of tissue activated (Reich et al., 2019; Soares et al., 2021), have been endowed with the ability to predict the efficacy of DBS surgery. Furthermore, some neuroimaging metrics have been considered as biomarkers for DBS outcomes. Raghu et al. (2021) found that the DTI-based connectivity between GPi and putamen correlated with clinical improvement. Through the cortical connectivity-based putaminal parcellations, they further discovered that the connectivity between the primary motor putamen and the posterior GPi limb could predict the GPi-DBS outcomes in cervical dystonia. Also, Gonzalez-Escamilla et al. (2019) proposed that the GM thickness of the regions where structural covariance network topology showed abnormality could significantly stratify the GPi-DBS therapeutic effects in generalized/cervical dystonic patients. However, these studies are almost all about GPi-DBS, and no neuroimaging biomarkers for STN-DBS outcomes exist. STN-DBS has been gradually dominating the neuromodulation for MS in terms of its advantages of visuality, lower power consumption, and higher symptom

improvement (Pandey and Sharma, 2017). Hence, in this article, we focus on STN-DBS only and define a promising GM biomarker for the first time.

Why can the mean GM volume of cluster 5 in the left lobule VIIIb predict the efficacy of STN-DBS surgery? It has been proved that STN stimulation can restore the short-latency intracortical inhibition and then lower cortical excitability (Cunic et al., 2002). We hypothesize that the cerebellar cortex (the left lobule VIIIb) participated in this process. To be specific, previous studies have investigated that STN has synaptic innervation to the cerebellar cortex via the relay of the pontine nuclei or the pedunculopontine nucleus in animals (Bostan et al., 2010; Bostan and Strick, 2018) and human brain (Lipp et al., 2022; Pelzer et al., 2013). And the output of the cerebellar cortex to the cerebrum is mainly the CTC pathway (Lipp et al., 2022; Nieuwhof et al., 2022). Thus, we hypothesize that the cerebellar cortex, as an intermediate node of this loop (STN-cerebellum-cerebrum), if atrophic, could limit the regulation of STN-DBS on CTC tract and then impede the decline of cortical excitability, thereby lowering the efficacy of STN-DBS. This hypothesis is in line with the finding of Fecikova et al. (2018) that the GM density of both cerebellar hemispheres (VIIb, VIII, IX, Crus II) inversely correlated with the mean short-latency intracortical inhibition in dystonic patients treated with GPi-DBS. Even though the stimulating targets were different, recent research demonstrated that STN-DBS and GPi-DBS worked through a largely overlapping network (Sobesky et al., 2022). To sum up, the GM volume of the cerebellar cortex can be informative about the DBS outcome.

4.5. Limitations and future work

Several limitations should be noted. Firstly, non-motor symptoms of MS have not been probed in the present article due to the lack of psychiatric, emotional, and cognitive evaluation. This makes it impossible to study the relationships between cerebellar GM changes and non-motor symptoms. Secondly, only the GM imaging was studied, and no diffusional or functional data were analyzed. Thirdly, the sample size of patients who had STN-DBS surgery was small, though the sample size of MS patients has been the largest so far. Finally, the prediction of DBS outcomes via GM metrics is exploratory and lacks external validation. Whether the mean GM volume of cluster 5 is a stable biomarker entails further in-depth investigations.

Therefore, future studies with a large-scale cohort, multimodal MRI metrics, and detailed clinical variables are warranted. Further, with the invention of MRI-compatible DBS stimulators, the comparative studies (pre-DBS vs post-DBS) are bound to facilitate the exploration of the pathophysiological foundation of MS and accelerate the disclosure of therapeutic mechanisms of DBS surgery for MS patients.

5. Conclusions

With a detailed focus on the cerebellum, we detected distinct GM atrophy in regions responsible for action observation, motor planning, visuospatial attention, and visual working memory in MS patients compared to HCs. Moreover, STN-DBS non-responders have lower GM volume in the left lobule VIIIb relative to STN-DBS responders. This GM reduction correlates with the symptom improvement rate after STN-DBS surgery. The GM volume in the left lobule VIIIb can not only distinguish MS patients from HCs but predict the STN-DBS outcomes with high accuracy. These findings facilitate our understanding of the intricate pathophysiology of MS and offer a reliable biomarker for MS diagnosis and DBS candidate selection before surgery.

Funding

This study was supported by the National Natural Science Foundation of China (No. 82001798 and No. 81871087), Chinese PLA General Hospital (No. LB20201A060004), China Brain Project (No. 2021ZD0200407).

CRediT authorship contribution statement

Bin Liu: Conceptualization, Methodology, Visualization, Writing – original draft. **Zhiqi Mao:** Resources, Data curation. **Zhiqiang Cui:** Resources. **Zhipei Ling:** Resources. **Xin Xu:** Resources. **Kunyu He:** Investigation. **Mengchu Cui:** Formal analysis. **Zhebin Feng:** Data curation. **Xinguang Yu:** Supervision, Project administration. **Yanyang Zhang:** Validation, Writing – review & editing, Funding acquisition.

Declaration of Competing Interest

The authors declare that they have no known competing financial interests or personal relationships that could have appeared to influence the work reported in this paper.

Data availability

Data will be made available on request.

Acknowledgement

We would thank all patients and healthy volunteers for their participation.

Appendix A. Supplementary data

Supplementary data to this article can be found online at https://doi.org/10.1016/j.nicl.2023.103316.

References

Argyelan, M., Carbon, M., Niethammer, M., Ulug, A.M., Voss, H.U., Bressman, S.B., Dhawan, V., Eidelberg, D., 2009. Cerebellothalamocortical connectivity regulates penetrance in dystonia. J. Neurosci. 29, 9740–9747. https://doi.org/10.1523/JNEUROSCI.2300-09.2009.

Ashburner, J., 2007. A fast diffeomorphic image registration algorithm. Neuroimage 38, 95–113. https://doi.org/10.1016/j.neuroimage.2007.07.007.

Ashburner, J., Friston, K.J., 2000. Voxel-based morphometry–the methods. Neuroimage 11, 805–821. https://doi.org/10.1006/nimg.2000.0582.

Battistella, G., Fuertinger, S., Fleysher, L., Ozelius, L.J., Simonyan, K., 2016. Cortical sensorimotor alterations classify clinical phenotype and putative genotype of spasmodic dysphonia. Eur. J. Neurol. 23, 1517–1527. https://doi.org/10.1111/ene.13067.

Battistella, G., Termsarasab, P., Ramdhani, R.A., Fuertinger, S., Simonyan, K., 2017. Isolated focal dystonia as a disorder of large-scale functional networks. Cereb. Cortex 27, 1203–1215. https://doi.org/10.1093/cercor/bhv313.

Berman, B.D., Honce, J.M., Shelton, E., Sillau, S.H., Nagae, L.M., 2018. Isolated focal dystonia phenotypes are associated with distinct patterns of altered microstructure. Neuroimage Clin. 19, 805–812. https://doi.org/10.1016/j.nicl.2018.06.004.

Bianchi, S., Fuertinger, S., Huddleston, H., Frucht, S.J., Simonyan, K., 2019. Functional and structural neural bases of task specificity in isolated focal dystonia. Mov. Disord. 34, 555–563. https://doi.org/10.1002/mds.27649.

Bologna, M., Berardelli, A., 2018. The cerebellum and dystonia. Handb. Clin. Neurol. 155, 259–272. https://doi.org/10.1016/B978-0-444-64189-2.00017-2.

Bostan, A.C., Dum, R.P., Strick, P.L., 2010. The basal ganglia communicate with the cerebellum. Proc. Natl. Acad. Sci. U. S. A. 107, 8452–8456. https://doi.org/10.1073/pnas.1000496107.

Bostan, A.C., Strick, P.L., 2018. The basal ganglia and the cerebellum: nodes in an integrated network. Nat. Rev. Neurosci. 19, 338–350. https://doi.org/10.1038/s41583-018-0002-7.

Brissenden, J.A., Levin, E.J., Osher, D.E., Halko, M.A., Somers, D.C., 2016. Functional evidence for a cerebellar node of the dorsal attention network. J. Neurosci. 36, 6083–6096. https://doi.org/10.1523/JNEUROSCI.0344-16.2016.

Brissenden, J.A., Somers, D.C., 2019. Cortico-cerebellar networks for visual attention and working memory. Curr. Opin. Psychol. 29, 239–247. https://doi.org/10.1016/j.copsyc.2019.05.003.

Brissenden, J.A., Tobyne, S.M., Osher, D.E., Levin, E.J., Halko, M.A., Somers, D.C., 2018. Topographic cortico-cerebellar networks revealed by visual attention and working memory. Curr. Biol. 28 (21), 3364–3372.e5.

Brissenden, J.A., Tobyne, S.M., Halko, M.A., Somers, D.C., 2021. Stimulus-Specific Visual Working Memory Representations in Human Cerebellar Lobule VIIb/VIIIa. J. Neurosci. 41, 1033–1045. https://doi.org/10.1523/JNEUROSCI.1253-20.2020.

Buckner, R.L., 2013. The cerebellum and cognitive function: 25 years of insight from anatomy and neuroimaging. Neuron 80, 807–815. https://doi.org/10.1016/j.neuron.2013.10.044.
Buckner, R.L., Krienen, F.M., Castellanos, A., Diaz, J.C., Yeo, B.T., 2011. The organization of the human cerebellum estimated by intrinsic functional connectivity. J. Neurophysiol. 106, 2322–2345. https://doi.org/10.1152/jn.00339.2011.
Burke, R.E., Fahn, S., Marsden, C.D., Bressman, S.B., Moskowitz, C., Friedman, J., 1985. Validity and reliability of a rating scale for the primary torsion dystonias. Neurology 35, 73–77. https://doi.org/10.1212/wnl.35.1.73.
Chirumamilla, V.C., Dresel, C., Koirala, N., Gonzalez-Escamilla, G., Deuschl, G., Zeuner, K.E., Muthuraman, M., Groppa, S., 2019. Structural brain network fingerprints of focal dystonia. Ther. Adv. Neurol. Disord. 12 https://doi.org/10.1177/1756286419880664.
Cunic, D., Roshan, L., Khan, F.I., Lozano, A.M., Lang, A.E., Chen, R., 2002. Effects of subthalamic nucleus stimulation on motor cortex excitability in Parkinson's disease. Neurology 58, 1665–1672. https://doi.org/10.1212/wnl.58.11.1665.
Diedrichsen, J., 2006. A spatially unbiased atlas template of the human cerebellum. Neuroimage 33, 127–138. https://doi.org/10.1016/j.neuroimage.2006.05.056.
Diedrichsen, J., Balsters, J.H., Flavell, J., Cussans, E., Ramnani, N., 2009. A probabilistic MR atlas of the human cerebellum. Neuroimage 46, 39–46. https://doi.org/10.1016/j.neuroimage.2009.01.045.
Fagan, M., Scorr, L., Bernhardt, D., Hess, E.J., Perlmutter, J.S., Pardo, C.A., Jinnah, H.A., 2021. Neuropathology of blepharospasm. Exp. Neurol. 346, 113855 https://doi.org/10.1016/j.expneurol.2021.113855.
Fang, T.C., Chen, C.M., Chang, M.H., Wu, C.H., Guo, Y.J., 2021. Altered Functional Connectivity and Sensory Processing in Blepharospasm and Hemifacial Spasm: Coexistence and Difference. Front. Neurol. 12, 759869 https://doi.org/10.3389/fneur.2021.759869.
Fecikova, A., Jech, R., Cejka, V., Capek, V., Stastna, D., Stetkarova, I., Mueller, K., Schroeter, M.L., Ruzicka, F., Urgosik, D., 2018. Benefits of pallidal stimulation in dystonia are linked to cerebellar volume and cortical inhibition. Sci. Rep. 8, 17218. https://doi.org/10.1038/s41598-018-34880-z.
Gonzalez-Escamilla, G., Muthuraman, M., Reich, M.M., Koirala, N., Riedel, C., Glaser, M., Lange, F., Deuschl, G., Volkmann, J., Groppa, S., 2019. Cortical network fingerprints predict deep brain stimulation outcome in dystonia. Mov. Disord. 34, 1537–1546. https://doi.org/10.1002/mds.27808.
Good, C.D., Johnsrude, I.S., Ashburner, J., Henson, R.N., Friston, K.J., Frackowiak, R.S., 2001. A voxel-based morphometric study of ageing in 465 normal adult human brains. Neuroimage 14, 21–36. https://doi.org/10.1006/nimg.2001.0786.
Hohenfeld, C., Werner, C.J., Reetz, K., 2018. Resting-state connectivity in neurodegenerative disorders: Is there potential for an imaging biomarker? Neuroimage Clin. 18, 849–870. https://doi.org/10.1016/j.nicl.2018.03.013.
Horisawa, S., Ochiai, T., Goto, S., Nakajima, T., Takeda, N., Kawamata, T., Taira, T., 2018. Long-term outcome of pallidal stimulation for Meige syndrome. J. Neurosurg. 130, 84–89. https://doi.org/10.3171/2017.7.JNS17323.
Hua, X., Zhang, B., Zheng, Z., Fan, H., Luo, L., Chen, X., Duan, J., Zhou, D., Li, M., Hong, T., Lu, G., 2020. Predictive factors of outcome in cervical dystonia following deep brain stimulation: an individual patient data meta-analysis. J. Neurol. 267, 1780–1792. https://doi.org/10.1007/s00415-020-09765-9.
Hutchinson, M., Nakamura, T., Moeller, J.R., Antonini, A., Belakhlef, A., Dhawan, V., Eidelberg, D., 2000. The metabolic topography of essential blepharospasm: a focal dystonia with general implications. Neurology 55, 673–677. https://doi.org/10.1212/wnl.55.5.673.
Isaias, I.U., Alterman, R.L., Tagliati, M., 2008. Outcome predictors of pallidal stimulation in patients with primary dystonia: the role of disease duration. Brain 131, 1895–1902. https://doi.org/10.1093/brain/awn120.
Jiang, W., Lei, Y., Wei, J., Yang, L., Wei, S., Yin, Q., Luo, S., Guo, W., 2019. Alterations of Interhemispheric Functional Connectivity and Degree Centrality in Cervical Dystonia: A Resting-State fMRI Study. Neural Plast. 2019, 7349894. https://doi.org/10.1155/2019/7349894.
Jinnah, H.A., Neychev, V., Hess, E.J., 2017. The anatomical basis for dystonia: the motor network model. Tremor Other Hyperkinet. Mov. (N. Y.) 7, 506. https://doi.org/10.7916/D8V69X3S.
Jochim, A., Li, Y., Gora-Stahlberg, G., Mantel, T., Berndt, M., Castrop, F., Dresel, C., Haslinger, B., 2018. Altered functional connectivity in blepharospasm/orofacial dystonia. Brain Behav 8 (1), e00894.
Khooshnoodi, M.A., Factor, S.A., Jinnah, H.A., 2013. Secondary blepharospasm associated with structural lesions of the brain. J. Neurol. Sci. 331, 98–101. https://doi.org/10.1016/j.jns.2013.05.022.
King, M., Hernandez-Castillo, C.R., Poldrack, R.A., Ivry, R.B., Diedrichsen, J., 2019. Functional boundaries in the human cerebellum revealed by a multi-domain task battery. Nat. Neurosci. 22, 1371–1378. https://doi.org/10.1038/s41593-019-0436-x.
Li, X., Lei, D., Niu, R., Li, L., Suo, X., Li, W., Yang, C., Yang, T., Ren, J., Pinaya, W.H.L., Zhou, D., Kemp, G.J., Gong, Q., 2021. Disruption of gray matter morphological networks in patients with paroxysmal kinesigenic dyskinesia. Hum. Brain Mapp. 42, 398–411. https://doi.org/10.1002/hbm.25230.
Lipp, I., Mole, J.P., Subramanian, L., Linden, D.E.J., Metzler-Baddeley, C., 2022. Investigating the anatomy and microstructure of the dentato-rubro-thalamic and subthalamo-ponto-cerebellar tracts in Parkinson's disease. Front. Neurol. 13, 793693 https://doi.org/10.3389/fneur.2022.793693.
Liu, J., Li, L., Chen, L., Liu, R., Jiang, Y., Fang, J., Wang, D., Liu, Z., Ouyang, J., 2020. Grey matter changes in Meige syndrome: a voxel-based morphology analysis. Sci. Rep. 10, 14533. https://doi.org/10.1038/s41598-020-71479-9.
Liu, J., Li, L., Li, Y., Wang, Q., Liu, R., Ding, H., 2021. Regional metabolic and network changes in Meige syndrome. Sci. Rep. 11, 15753. https://doi.org/10.1038/s41598-021-95333-8.
Luo, Y., Guo, Y., Zhong, L., Liu, Y., Dang, C., Wang, Y., Zeng, J., Zhang, W., Peng, K., Liu, G., 2022. Abnormal dynamic brain activity and functional connectivity of primary motor cortex in blepharospasm. Eur. J. Neurol. 29, 1035–1043. https://doi.org/10.1111/ene.15233.
Ma, H., Qu, J., Ye, L., Shu, Y., Qu, Q., 2021. Blepharospasm, Oromandibular Dystonia, and Meige Syndrome: Clinical and Genetic Update. Front. Neurol. 12, 630221 https://doi.org/10.3389/fneur.2021.630221.
Malone, A., Manto, M., Hass, C., 2014. Dissecting the links between cerebellum and dystonia. Cerebellum 13, 666–668. https://doi.org/10.1007/s12311-014-0601-4.
Mantel, T., Jochim, A., Meindl, T., Deppe, J., Zimmer, C., Li, Y., Haslinger, B., 2022. Thalamic structural connectivity profiles in blepharospam/Meige's syndrome. Neuroimage Clin. 34, 103013 https://doi.org/10.1016/j.nicl.2022.103013.
Martino, D., Di Giorgio, A., D'Ambrosio, E., Popolizio, T., Macerollo, A., Livrea, P., Bertolino, A., Defazio, G., 2011. Cortical gray matter changes in primary blepharospasm: a voxel-based morphometry study. Mov. Disord. 26, 1907–1912. https://doi.org/10.1002/mds.23724.
Middleton, F.A., Strick, P.L., 1994. Anatomical evidence for cerebellar and basal ganglia involvement in higher cognitive function. Science 266, 458–461. https://doi.org/10.1126/science.7939688.
Morigaki, R., Miyamoto, R., Matsuda, T., Miyake, K., Yamamoto, N., Takagi, Y., 2021. Dystonia and Cerebellum: From Bench to Bedside. Life (Basel) 11, 776. https://doi.org/10.3390/life11080776.
Neumann, W.J., Horn, A., Ewert, S., Huebl, J., Brucke, C., Slentz, C., Schneider, G.H., Kuhn, A.A., 2017. A localized pallidal physiomarker in cervical dystonia. Ann. Neurol. 82, 912–924. https://doi.org/10.1002/ana.25095.
Nguyen, P., Kelly, D., Glickman, A., Argaw, S., Shelton, E., Peterson, D.A., Berman, B.D., 2020. Abnormal Neural Responses During Reflexive Blinking in Blepharospasm: An Event-Related Functional MRI Study. Mov. Disord. 35, 1173–1180. https://doi.org/10.1002/mds.28042.
Nieuwhof, F., Toni, I., Dirkx, M.F., Gallea, C., Vidailhet, M., Buijink, A.W.G., van Rootselaar, A.F., van de Warrenburg, B.P.C., Helmich, R.C., 2022. Cerebello-thalamic activity drives an abnormal motor network into dystonic tremor. Neuroimage Clin 33, 102919. https://doi.org/10.1016/j.nicl.2021.102919.
Obermann, M., Yaldizli, O., De Greiff, A., Lachenmayer, M.L., Buhl, A.R., Tumczak, F., Gizewski, E.R., Diener, H.C., Maschke, M., 2007. Morphometric changes of sensorimotor structures in focal dystonia. Mov. Disord. 22, 1117–1123. https://doi.org/10.1002/mds.21495.
Pan, P., Wei, S., Ou, Y., Jiang, W., Li, W., Lei, Y., Liu, F., Guo, W., Luo, S., 2019. Reduced global-brain functional connectivity and its relationship with symptomatic severity in cervical dystonia. Front. Neurol. 10, 1358. https://doi.org/10.3389/fneur.2019.01358.
Pan, P., Wei, S., Li, H., Ou, Y., Liu, F., Jiang, W., Li, W., Lei, Y., Tang, Y., Guo, W., Luo, S., Su, J., 2021. Voxel-wise brain-wide functional connectivity abnormalities in patients with primary blepharospasm at rest. Neural Plast. 2021, 1–9.
Pandey, S., Sharma, S., 2017. Meige's syndrome: History, epidemiology, clinical features, pathogenesis and treatment. J. Neurol. Sci. 372, 162–170. https://doi.org/10.1016/j.jns.2016.11.053.
Pauls, K.A.M., Krauss, J.K., Kampfer, C.E., Kuhn, A.A., Schrader, C., Sudmeyer, M., Allert, N., Benecke, R., Blahak, C., Boller, J.K., Fink, G.R., Fogel, W., Liebig, T., El Majdoub, F., Mahlknecht, P., Kessler, J., Mueller, J., Voges, J., Wittstock, M., Wolters, A., Maarouf, M., Moro, E., Volkmann, J., Bhatia, K.P., Timmermann, L., 2017. Causes of failure of pallidal deep brain stimulation in cases with pre-operative diagnosis of isolated dystonia. Parkinsonism Relat. Disord. 43, 38–48. https://doi.org/10.1016/j.parkreldis.2017.06.023.
Pelzer, E.A., Hintzen, A., Goldau, M., von Cramon, D.Y., Timmermann, L., Tittgemeyer, M., 2013. Cerebellar networks with basal ganglia: feasibility for tracking cerebello-pallidal and subthalamo-cerebellar projections in the human brain. Eur. J. Neurosci. 38, 3106–3114. https://doi.org/10.1111/ejn.12314.
Piccinin, C.C., Piovesana, L.G., Santos, M.C., Guimaraes, R.P., De Campos, B.M., Rezende, T.J., Campos, L.S., Torres, F.R., Amato-Filho, A.C., Franca Jr., M.C., Lopes-Cendes, I., Cendes, F., D'Abreu, A., 2014a. Diffuse decreased gray matter in patients with idiopathic craniocervical dystonia: a voxel-based morphometry study. Front. Neurol. 5, 283. https://doi.org/10.3389/fneur.2014.00283.
Piccinin, C.C., Santos, M.C., Piovesana, L.G., Campos, L.S., Guimaraes, R.P., Campos, B.M., Torres, F.R., Franca, M.C., Amato-Filho, A.C., Lopes-Cendes, I., Cendes, F., D'Abreu, A., 2014b. Infratentorial gray matter atrophy and excess in primary craniocervical dystonia. Parkinsonism Relat. Disord. 20, 198–203. https://doi.org/10.1016/j.parkreldis.2013.10.026.
Pinheiro, G.L., Guimaraes, R.P., Piovesana, L.G., Campos, B.M., Campos, L.S., Azevedo, P.C., Torres, F.R., Amato-Filho, A.C., Franca Jr., M.C., Lopes-Cendes, I., Cendes, F., D'Abreu, A., 2015. White matter microstructure in idiopathic craniocervical dystonia. Tremor Other Hyperkinet. Mov. (N. Y.) 5. https://doi.org/10.7916/D86972H6.
Pizoli, C.E., Jinnah, H.A., Billingsley, M.L., Hess, E.J., 2002. Abnormal cerebellar signaling induces dystonia in mice. J. Neurosci. 22 (17), 7825–7833.
Popa, T., Velayudhan, B., Hubsch, C., Pradeep, S., Roze, E., Vidailhet, M., Meunier, S., Kishore, A., 2013. Cerebellar processing of sensory inputs primes motor cortex plasticity. Cereb. Cortex 23, 305–314. https://doi.org/10.1093/cercor/bhs016.
Prudente, C.N., Pardo, C.A., Xiao, J., Hanfelt, J., Hess, E.J., Ledoux, M.S., Jinnah, H.A., 2013. Neuropathology of cervical dystonia. Exp. Neurol. 241, 95–104. https://doi.org/10.1016/j.expneurol.2012.11.019.
Raghu, A.L.B., Eraifej, J., Sarangmat, N., Stein, J., FitzGerald, J.J., Payne, S., Aziz, T.Z., Green, A.L., 2021. Pallido-putaminal connectivity predicts outcomes of deep brain

stimulation for cervical dystonia. Brain 144, 3589–3596. https://doi.org/10.1093/brain/awab280.
Ramdhani, R.A., Kumar, V., Velickovic, M., Frucht, S.J., Tagliati, M., Simonyan, K., 2014. What's special about task in dystonia? A voxel-based morphometry and diffusion weighted imaging study. Mov. Disord. 29, 1141–1150. https://doi.org/10.1002/mds.25934.
Reich, M.M., Horn, A., Lange, F., Roothans, J., Paschen, S., Runge, J., Wodarg, F., Pozzi, N.G., Witt, K., Nickl, R.C., Soussand, L., Ewert, S., Maltese, V., Wittstock, M., Schneider, G.H., Coenen, V., Mahlknecht, P., Poewe, W., Eisner, W., Helmers, A.K., Matthies, C., Sturm, V., Isaias, I.U., Krauss, J.K., Kuhn, A.A., Deuschl, G., Volkmann, J., 2019. Probabilistic mapping of the antidystonic effect of pallidal neurostimulation: a multicentre imaging study. Brain 142, 1386–1398. https://doi.org/10.1093/brain/awz046.
Romano, R., Bertolino, A., Gigante, A., Martino, D., Livrea, P., Defazio, G., 2014. Impaired cognitive functions in adult-onset primary cranial cervical dystonia. Parkinsonism Relat. Disord. 20, 162–165. https://doi.org/10.1016/j.parkreldis.2013.10.008.
Schouten, T.M., Koini, M., de Vos, F., Seiler, S., van der Grond, J., Lechner, A., Hafkemeijer, A., Moller, C., Schmidt, R., de Rooij, M., Rombouts, S., 2016. Combining anatomical, diffusion, and resting state functional magnetic resonance imaging for individual classification of mild and moderate Alzheimer's disease. Neuroimage Clin. 11, 46–51. https://doi.org/10.1016/j.nicl.2016.01.002.
Soares, C., Reich, M.M., Costa, F., Lange, F., Roothans, J., Reis, C., Vaz, R., Rosas, M.J., Volkmann, J., 2021. Predicting Outcome in a Cohort of Isolated and Combined Dystonia within Probabilistic Brain Mapping. Mov. Disord. Clin. Pract. 8, 1234–1239. https://doi.org/10.1002/mdc3.13345.
Sobesky, L., Goede, L., Odekerken, V.J.J., Wang, Q., Li, N., Neudorfer, C., Rajamani, N., Al-Fatly, B., Reich, M., Volkmann, J., de Bie, R.M.A., Kuhn, A.A., Horn, A., 2022. Subthalamic and pallidal deep brain stimulation: are we modulating the same network? Brain 145, 251–262. https://doi.org/10.1093/brain/awab258.
Tian, H., Zhang, B., Yu, Y., Zhen, X., Zhang, L., Yuan, Y., Wang, L., 2021. Electrophysiological signatures predict clinical outcomes after deep brain stimulation of the globus pallidus internus in Meige syndrome. Brain Stimul. 14, 685–692. https://doi.org/10.1016/j.brs.2021.04.005.
Tomic, A., Agosta, F., Sarasso, E., Svetel, M., Kresojevic, N., Fontana, A., Canu, E., Petrovic, I., Kostic, V.S., Filippi, M., 2021. Brain Structural Changes in Focal Dystonia-What About Task Specificity? A Multimodal MRI Study. Mov. Disord. 36, 196–205. https://doi.org/10.1002/mds.28304.
Vagefi, M.R., Lin, C.C., McCann, J.D., Anderson, R.L., 2008. Exacerbation of blepharospasm associated with craniocervical dystonia after placement of bilateral globus pallidus internus deep brain stimulator. Mov. Disord. 23, 454–456. https://doi.org/10.1002/mds.21889.
Valls-Sole, J., Defazio, G., 2016. Blepharospasm: Update on Epidemiology, Clinical Aspects, and Pathophysiology. Front. Neurol. 7, 45. https://doi.org/10.3389/fneur.2016.00045.
Voogd, J., 2003. The human cerebellum. J. Chem. Neuroanat. 26, 243–252. https://doi.org/10.1016/j.jchemneu.2003.07.005.
Wang, X., Mao, Z., Cui, Z., Xu, X., Pan, L., Liang, S., Ling, Z., Yu, X., 2019a. Predictive factors for long-term clinical outcomes of deep brain stimulation in the treatment of primary Meige syndrome. J. Neurosurg. 132, 1367–1375. https://doi.org/10.3171/2019.1.JNS182555.
Wang, X., Zhang, Z., Mao, Z., Yu, X., 2019b. Deep brain stimulation for Meige syndrome: a meta-analysis with individual patient data. J. Neurol. 266, 2646–2656. https://doi.org/10.1007/s00415-019-09462-2.
White, J.J., Sillitoe, R.V., 2017. Genetic silencing of olivocerebellar synapses causes dystonia-like behaviour in mice. Nat Commun 8, 14912. https://doi.org/10.1038/ncomms14912.
Xue, A., Kong, R., Yang, Q., Eldaief, M.C., Angeli, P.A., DiNicola, L.M., Braga, R.M., Buckner, R.L., Yeo, B.T.T., 2021. The detailed organization of the human cerebellum estimated by intrinsic functional connectivity within the individual. J. Neurophysiol. 125, 358–384. https://doi.org/10.1152/jn.00561.2020.
Yang, J., Luo, C., Song, W., Guo, X., Zhao, B., Chen, X., Huang, X., Gong, Q., Shang, H.F., 2014. Diffusion tensor imaging in blepharospasm and blepharospasm-oromandibular dystonia. J. Neurol. 261, 1413–1424. https://doi.org/10.1007/s00415-014-7359-y.
Yao, C., Horn, A., Li, N., Lu, Y., Fu, Z., Wang, N., Aziz, T.Z., Wang, L., Zhang, S., 2019. Post-operative electrode location and clinical efficacy of subthalamic nucleus deep brain stimulation in Meige syndrome. Parkinsonism Relat. Disord. 58, 40–45. https://doi.org/10.1016/j.parkreldis.2018.05.014.
Zhan, S., Sun, F., Pan, Y., Liu, W., Huang, P., Cao, C., Zhang, J., Li, D., Sun, B., 2018. Bilateral deep brain stimulation of the subthalamic nucleus in primary Meige syndrome. J. Neurosurg. 128, 897–902. https://doi.org/10.3171/2016.12.JNS16383.
Zheng, Z., Pan, P., Wang, W., Shang, H., 2012. Neural network of primary focal dystonia by an anatomic likelihood estimation meta-analysis of gray matter abnormalities. J. Neurol. Sci. 316, 51–55. https://doi.org/10.1016/j.jns.2012.01.032.
Zhou, B., Wang, J., Huang, Y., Yang, Y., Gong, Q., Zhou, D., 2013. A resting state functional magnetic resonance imaging study of patients with benign essential blepharospasm. J. Neuroophthalmol. 33, 235–240. https://doi.org/10.1097/WNO.0b013e31828f69e5.
Zhu, G., Geng, X., Tan, Z., Chen, Y., Zhang, R., Wang, X., Aziz, T., Wang, S., Zhang, J., 2018. Characteristics of Globus pallidus internus local field potentials in hyperkinetic disease. Front. Neurol. 9, 934. https://doi.org/10.3389/fneur.2018.00934.

Further reading

Delmaire, C., Vidailhet, M., Elbaz, A., Bourdain, F., Bleton, J.P., Sangla, S., Meunier, S., Terrier, A., Lehericy, S., 2007. Structural abnormalities in the cerebellum and sensorimotor circuit in writer's cramp. Neurology 69, 376–380. https://doi.org/10.1212/01.wnl.0000266591.49624.1a.